Angle tunable trapped mode in a THz metamaterial

Bagvanth Reddy Sangala[a], Harshad Surdi[b], Prathmesh Deshmukh[b], Goutam Rana[c],
Venu Gopal Achanta[b] & S S Prabhu[b]*

[a]Department of Physics, PG Center at Wanaparthy, Palamuru University,
Wanaparthy 509 103, India

[b]Department of Condensed Matter Physics, Tata Institute of Fundamental Research,
Colaba 400 005, India

[c]Department of Electrical Engineering, Indian Institute of Technology, Mumbai,
Pawai 400 076, India

We report trapped mode in Fano-like resonance in a terahertz (THz) metameterial (MM) consisting of a concentric circular and elliptical gold rings on semi-insulating GaAs substrate. We present the finite element method (FEM) based design, electron beam lithography based fabrication and 0.2-2 THz window spectroscopic results. The trapped mode of the MM can be tuned by the angle between the major axis of the ellipse and the polarization of incident THz electric field (maximum amplitude ~100V/m).

1 Introduction

The asymmetric resonant line profile in a spectrum, called Fano-resonance arises due to interaction of systems with a continuum and discrete lines in natural or artificial media[1-3]. Metamaterials are artificial materials made up of metallo-dielectric sub-wavelength constituents. These can show exotic properties like hyper resolution, invisibility cloaking, negative refraction, giant chirality, etc[4]. At first, a 2D metamaterial with translational unit cell having asymmetric split ring resonator showed a trapped mode with a Fano-like resonance due to interaction between a sub-radiant mode and a super-radiant mode[5]. Subsequently, the Fano-like resonance with trapped modes in metamaterials was shown to be useful for narrowband tunable filters[6], enhancement of quantum dot luminescence[7], lasing spaser[8], bio-molecular sensing[9], electro-optic switching[10], slowing light[11], thin film thickness sensing[9,12,13]directional dependent transmission[14], refractive index change sensing[13], etc. While some of these structures showing Fano-like resonances have asymmetric shaped unit cells[9-11,14], metamaterials with symmetric unit cells also were reported[15,16]. Fano-like resonance was also realized in quasi-3D (multilayer) metamaterials[17,18]. In addition to these, Fano-like resonance was also observed in plasmonic waveguides[19,20], graphene-metal grating structures[21], metallic nano shells[22-24], concentric or nonconcentric ring and discs[24-25], two-beam interference in a micro cavity[27], etc. Metamaterials with Fano-like resonance have been studied in terahertz (THz) regime also[2,3,11,13,14,16,27-32]. In view of the exciting potential applications of the Fano-like resonance with trapped modes in materials, tunability of (or control over) the resonance will be of great use.

Tuning of the Fano-like resonance was reported by tuning the geometrical dimensions of the constituents of the material[5,20,23,25,33], by temperature tuning of superconducting metamaterials[34,] by laser irradiation of a non-linear optical material[35,36], laser induced phase change of a material[17], DC induced phase change of a material[10], temperature tuning of a microringplasmonic resonator[26], angle tuning of a plasmonic ring or disc cavities[27,25]. We report a THz metamaterial with anangle tunable trapped mode in Fano-like resonance in this work. The uniqueness of this metamaterial is that just by physical rotation of the metamaterial sample holder, one can tune the Fano-like resonance. The unit cell of the metamaterial consists of concentric circular and elliptical gold pads on a semi-insulating Gallium Arsenide (SI-GaAs). As the metamaterial is rotated, that is, as the angle between the major axis of the ellipse and the incident

_____

*Corresponding author (E-mail: prabhu@tifr.res.in)

THz electric field changes, the trapped mode frequency shifts from 0.95 THz to 1.1 THz.

2 Designing, Fabrication and Characterization

The transmission of THz radiation through the metamaterial is simulated using the finite element method based software, COMSOL multiphysics. The schematic of the unit cell of the metamaterial is shown in Fig. 1(a). It has concentric circular and elliptical gold ring pads on SI-GaAs substrate. The outer diameter of the circular ring is 40 µm. The outer major and minor axes of the elliptical ring are 34 µm and 28 µm, respectively. The width and height of both the ring sare 2 µm and 150 nm, respectively.

The angle between the major axis of the ellipse and electric field of incident THz is measured as θ.

In computation, periodic boundary conditions are applied to the transverse directions of the unit cell. The THz radiation is shown at normal incidence on the metamaterial. The wave vector was set as:

$$\vec{k} = \frac{2\pi}{\lambda}\hat{z}$$

and the electric and magnetic fields were given by:

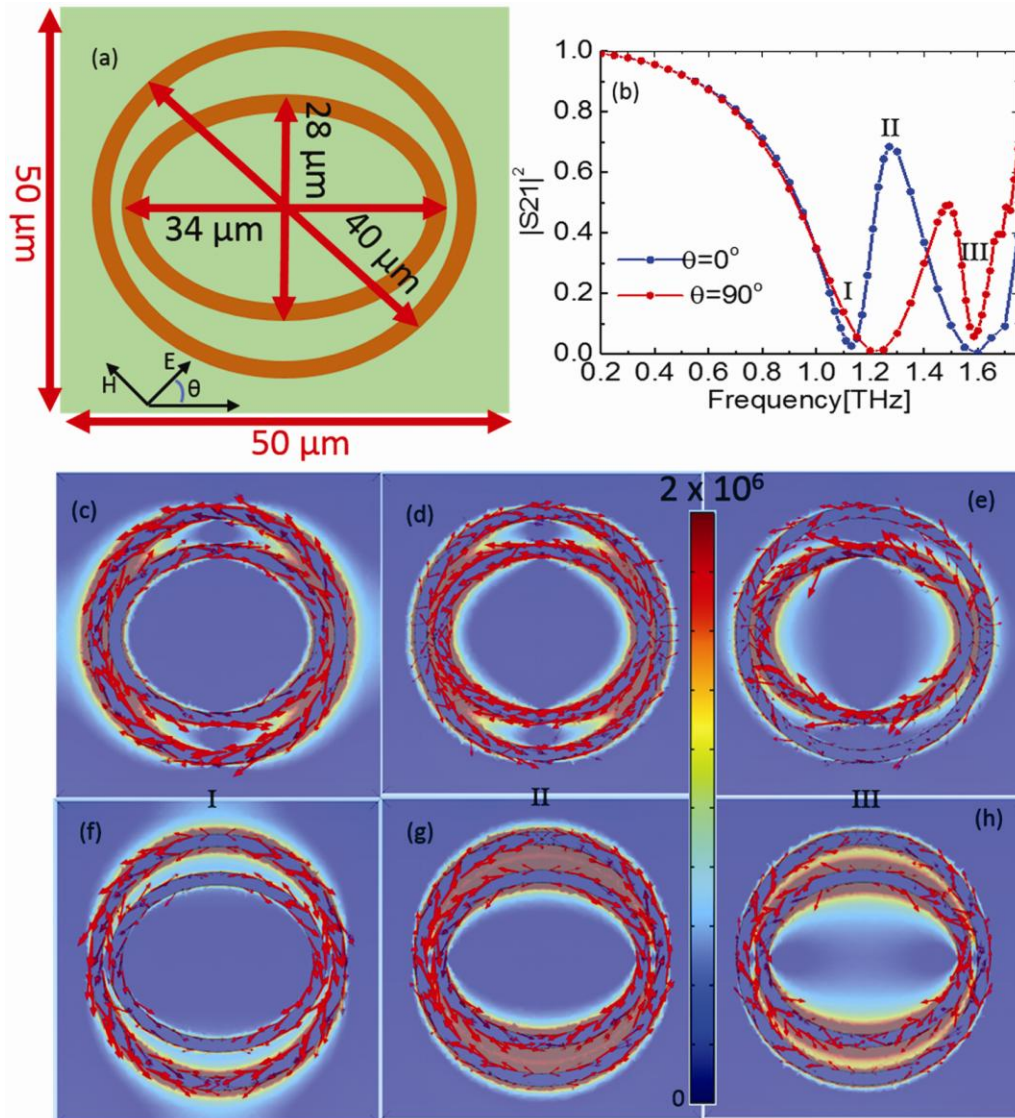$$\vec{E} = \left(\cos\theta\hat{x} + \sin\theta\hat{y}\right)\exp\left(i\vec{k}\cdot\vec{r}\right).$$

Fig. 1 — (a) Unit cell of the metamaterial: gold pads of width 2 µm and height 150 nm on semi-insulating gallium arsenide and (b) normalized $|S21|^2$ versus frequency for angle θ=0° and 90°. Electric field norm color plot, current density arrow plot at extrema before trapped mode (I), at trapped mode peak (II), and after trapped mode (III) for θ=0°, respectively in (c), (d), (e) and that for θ =90° in (f), (g), (h).

$$\vec{B} = \vec{k} \times \vec{E}.$$

In the design, *x*-axis is the major axis of the ellipse. The scattering parameters are calculated for various frequencies of the THz and $|S21|^2$ versus frequency is plotted to see the power transmission. Figure 1(b) shows the trapped mode peaks at 1.2 and 1.5 THz in the $|S21|^2$ versus frequency data for θ=0° and 90°, respectively. This difference could be due to change of dipole resonance of inner (elliptical) ring for angle 0° and 90°. Here, I, II, and III show the extreme before trapped mode, at trapped mode peak, and after trapped mode, respectively. Figure 1(c, d,e) shows the electric field norm (color) and current density direction (arrow) of modes at I (1.13 THz), II (1.27 THz), and III (1.55 THz) for theta=0°. In Fig.1(c) we observe that the electric dipole moment due to outer ring's currents is larger than that of the inner ring resulting in a radiative mode. In Fig. 1(d), we see that the electric dipoles due to inner and outer ring are almost same resulting in a non-radiative trapped mode. In fig. 1(e), the electric dipole moment of the outer ring is cancelled and only that of the inner ring exists resulting in a highly radiative mode. Figure 1 (f,g,h) show the electric field norm and current density direction of modes at I (1.2 THz), II (1.495 THz), and III (1.585 THz) for θ=90°. Figure 1(f) shows that the dipole moment due to the inner ring is almost cancelled and the dipole moment of the outer ring exists giving rise to a highly radiative mode. In Fig. 1(g), the equal and out of phase electric dipoles due to the outer and inner rings cancel out giving rise to a trapped mode. In Fig 1(h), the outer ring dipole moment is weaker than that of the inner ring giving rise to a radiative mode. This is in contrast to the case of two concentric circular rings[15], where the dipole moments of both the rings were present in I, II, and III but in our case, in Fig. 1(e, f) we can see one of the dipole moments is cancelled and the other dipole moment was resulting in highly radiative modes.

The designed metamaterial is fabricated by electron beam lithography. An SI-GaAs substrate was baked at 200 °C, spin coated with 200 nm thick PMMA electron beam resist, baked at 170 °C for 6 min. The sample was written by electron beam in 5×5 mm^2 area, developed in a solution and stopper. It was DC sputtered with gold, and lifted off in an acetone bath using sonication process to get the gold pads on SI-GaAs. Figure 2(a) shows an SEM image of the unit cell of the metamaterial. This sample was mounted on a rotatable mount in a THz-TDS setup. THz

waveforms before mounting the sample (reference scan) and at various angles through the mounted sample (sample scans) were acquired. Figure 2(b) shows the reference and sample waveforms for θ=0° and 90°. The waveforms were truncated before the echo from the SI-GaAs substrate and the Fourier transforms were calculated. The square of the ratio of the sample spectrum and the reference spectrum, power transmission coefficient, is shown in Fig. 2(c) when the sample is at θ=0° and 90° orientations. We can see the trapped mode peak at 0.95 THz and 1.1 THz for angle 0° and 90°. The variation in the theoretical and trapped mode frequency could be due to the fact that we did not take dispersion of gold or SI-GaAs into consideration in the simulations. Figure 3 shows the contour plot of experimental power transmission versus frequency for various angles between 0 and 90°. We can see the shift in the trapped mode peak (indicated by a solid black line to guide the eye) from 0.95 THz to 1.1 THz as the angle changes from 0° to 90°.
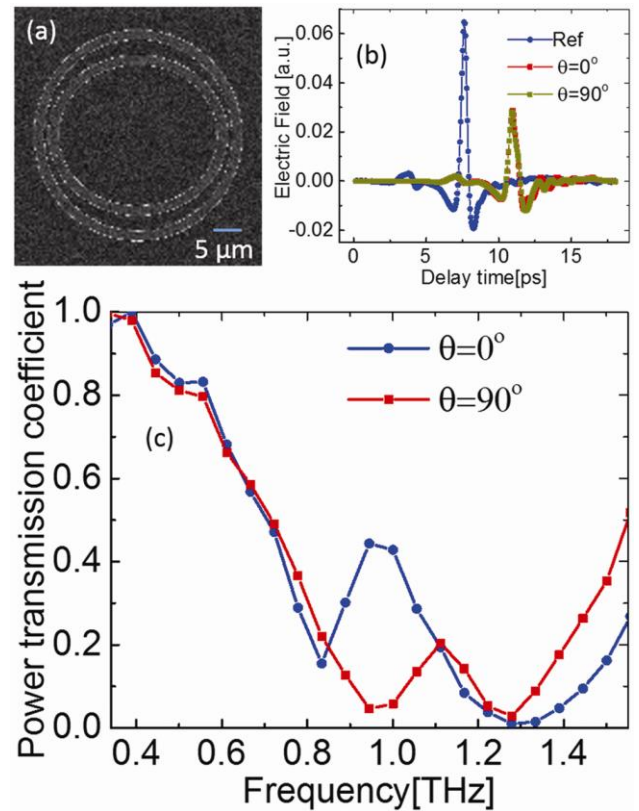

Fig. 2 — (a) SEM image of the fabricated metamaterial unit cell, (b) THz waveforms transmitted through the reference and the metamaterial at angles 0° and 90° and (c) experimental power transmission coefficient versus frequency for angles 0° and 90° of the metamaterial.
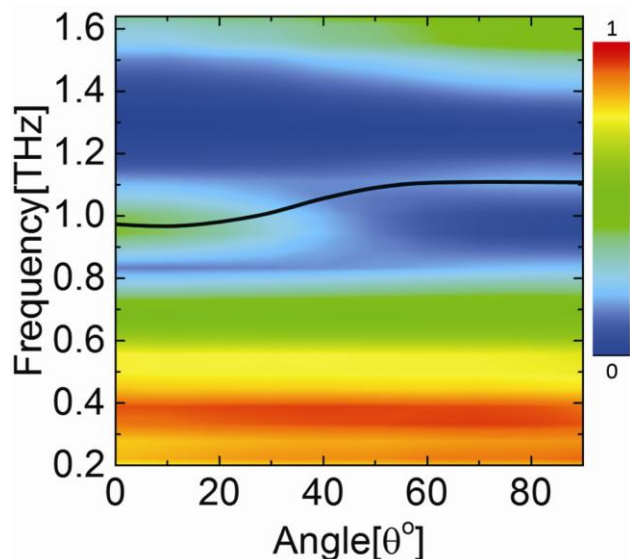
Fig. 3 — Experimental normalized power transmission coefficient versus frequency for angles between 0° and 90°. The thick black line traces the trapped mode peak position.

3 Conclusions

We report angle tunable trapped mode in a concentric circular-elliptical metamaterial. The metamaterial was fabricated by electron beam lithography and characterized by THz-TDS. The finite element method simulations revealed the origin of the trapped mode to be due to interference dipole modes of the rings. As the angle of the metamaterial with respect to the normally incident THz electric field changes from 0° to 90°, the trapped mode peak changes from 0.95 THz to 1.1 THz.

References

1   Lukyanchuk B, Zheludev N I, Maier S A, Halas N J, Nordlander P, Harald G & Chong T, *Nat Mater*, 9 (2010) 707.
2   Al-Naib Ibraheem, Jansen C, Singh R, Walther M, & Koch M, *IEEE Trans Terahertz Sci Technol*, 3 (2013) 772.
3   Singh Ranjan, Al-Naib Ibraheem, Cao W, Rockstuhl C, Koch M & Zhang W, *IEEE Trans Terahertz Sci Technol*, 3 (2013) 820.
4   Liu L & Zhang X, *Chem Soc Rev*, 40 (2011) 2494.
5   Fedotov V A, Rose M, Prosvirnin S L, Papasimakis N & Zheludev N I, *Phys Rev Lett*, 99 (2007) 147401.
6   Zheludev N I, Plum E & Fedotov V A, *Appl Phys Lett*, 99 (2011) 171915.
7   Tanaka K, Plum E, Ou J Y, Uchino T & Zheludev N I, *Phys Rev Lett*, 105 (2010) 227403.
8   Zheludev N I, Prosvirnin S L, Papasimakis N & Fedotov V A, *Nat Photonics*, 2 (2008) 351.
9   Wu C, Khanikaev A B, Adato R, Arju N, Yanik A A, Altug H & Shvets G, *Nat Mater*, 11 (2012) 69.
10   Samson Z L, MacDonald K F, Angelis F D, Gholipour B, Knight K, Huang C C, Fabrizio E D, Hewak D W & Zheludev N I, *Appl Phys Lett*, 96 (2010) 143105.
11   Zhang S, Dentcho, Genov A, Wang Y, Liu M, & Zhang X, *Phys Rev Lett*, 101(2008) 047401.
12   Ibraheem A, Al-Naib I, Jansen C, & Koch M, *Appl Phys Lett*, 93 (2008) 083507.
13   Singh Ranjan, Cao Wei, AI-Naib I, Longqingcong, Withayachumnankul W & Zhang W, *Appl Phys Lett*, 105 (2014) 171101.
14   Singh Ranjan, Plum E, C Menzel, Rockstuhl C, Azad A K, Cheville R A, Lederer F, Zhang W & Zheludev N I, *Phys Rev B*, 80 (2009) 153104.
15   Papasimakis N, Fu Y H, Fedotov V A, Prosvirnin S L, Tsai D P, & Zheludev N I, *Appl Phys Lett*, 94 (2009) 211902.
16   Shu J, Gao W, Reichel K, Nickel D, Dominguez J, Brener I, Mittleman D M, & Xu Q, *Opt Express*, 22 (2014) 3753.
17   Cao T, Wei C, Simpson R E, Zhang L, & Cryan M J, *Sci Rep*, 14 (2014) 4463.
18   Kanjanasit K & Wang C H, *Appl Phys Lett*, 102 (2013) 251108.
19   Qi J, Chen Z, Chen J, Li Y, Qiang W, Xu J, & Sun Q, *Opt Express*, 22 (2014) 14688.
20   Chen Zhao, Hu R, Cui L, Yu L, Wang L & Xiao J, *Opt Commun*, 320 (2014) 6.
21   Chen Z X, Chen J H, Wu Z J, Hu W, Zhang X J & Lu Y Q, *Appl Phys Lett*, 104 (2014) 161114.
22   Wu D, Jiang S M & Xiao L J, *J Phys Chem C*, 115 (2011) 23797.
23   Pena-Rodriguez O, Rivera A, Campoy-Quiles M & Pal U, *Nanoscale*, 5 (2013) 209.
24   Ho J F, Lukyanchuk B & Zhang J B, *Appl Phys A*, 107 (2012) 133.
25   Hao F, Yannick S, Dorpe P V, Maier S A, Halas N J & Nordlander P, *Nano Lett*, 8 (2008) 3983.
26   Hu T, Yu P, Qiu C, Qiu H, Wang F, Yang M, Jiang X, Yu H &Yang J, *Appl Phys Lett*, 102 (2013) 011112.
27   Hao F, Nordlander P, Sonnefraud Y, Dorpe P V & Maier S A, *ACS Nano*, 3 (2009) 643.
28   Singh Ranjan, AI-Naib Ibraheem, Koch M & Zhang W, *Opt Express*, 19 (2011) 6312.
29   Cao W, Singh R, AI-Naib I A I, He M, Taylor A J & Zhang W, *Opt Lett*, 37 (2012) 3366.
30   Singh Ranjan, Al-Naib I A I, Koch M, & Zhang W, *Opt Express*, 18 (2010) 13044.
31   Singh R, Al-Naib I A I, Yang Y, Chowdhury D R, Cao W, Rockstuhl C, Ozaki T, Morandotti R & Zhang W, *Appl Phys Lett*, 99 (2011) 201107.
32   Xiao X, Wu J, Miyamaru F, Zhang M, Li S, Takeda M W, Wen W & Sheng P, *Appl Phys Lett*, 98 (2011) 011911.
33   Zhang F, Hu X, Zhu Y, Fu Y, Yand Hong & Gong Q, *Appl Phys Lett*, 102 (2013) 181109.
34   Zhang Y, Hu Xi, Fu Y, Yang H & Gong Q, *Appl Phys Lett*, 100 (2012) 031106.
35   Sun B, Zhao L, Chao W, Yi X, Liu Z, Wang G & Li J, *J Phys Chem C*, 118 (2014) 25124.
36   Fedotov V A, Tsiatmas A, Shi J H, Buckingham R, Groot P de, Chen Y, Wang S & Zheludev N I, *Opt Express*, 18 (2010) 9015.